Asymmetric Coordination Induces Electron Localization at Ca Sites for Robust CO$_2$ Electroreduction to CO

Qiyou Wang, Minyang Dai, Hongmei Li, Ying-Rui Lu, Ting-Shan Chan, Chao Ma, Kang Liu, Junwei Fu, Wanru Liao, Shanyong Chen, Evangelina Pensa, Ye Wang, Shiguo Zhang, Yifei Sun,* Emiliano Cortés,* and Min Liu*

Main group single atom catalysts (SACs) are promising for CO$_2$ electroreduction to CO by virtue of their ability in preventing the hydrogen evolution reaction and CO poisoning. Unfortunately, their delocalized orbitals reduce the CO$_2$ activation to *COOH. Herein, an O doping strategy to localize electrons on p-orbitals through asymmetric coordination of Ca SAC sites (Ca-N$_3$O) is developed, thus enhancing the CO$_2$ activation. Theoretical calculations indicate that asymmetric coordination of Ca-N$_3$O improves electron-localization around Ca sites and thus promotes *COOH formation. X-ray absorption fine spectroscopy shows the obtained Ca-N$_3$O features: one O and three N coordinated atoms with one Ca as a reactive site. In situ attenuated total reflection infrared spectroscopy proves that Ca-N$_3$O promotes *COOH formation. As a result, the Ca-N$_3$O catalyst exhibits a state-of-the-art turnover frequency of ≈15 000 per hour in an H-cell and a large current density of −400 mA cm^{-2} with a CO Faradaic efficiency (FE) ≥ 90% in a flow cell. Moreover, Ca-N$_3$O sites retain a FE above 90% even with a 30% diluted CO$_2$ concentration.

1. Introduction

CO$_2$ electroreduction reaction (CO$_2$RR) to CO has aroused widespread attention, because it represents a promising solution for mitigation of excessive CO$_2$ concentration, meanwhile providing a feedstock to Fischer-Tropsch synthesis.[1]

As is well-known, single atom catalysts (SACs) possess unambiguous active sites and maximize atom utilization, which are deemed as a candidate for CO production.[2] To date, the development of traditional d-block SACs for CO$_2$RR is seriously hindered,[3] because their d-orbitals bring about the strong adsorption of *H and *CO resulting in severe hydrogen evolution (HER) and CO poisoning.[4] Oppositely, main group SACs show a great potential for CO$_2$ electroreduction (CO$_2$RR) to CO due to their robust ability in restraining adsorption of *H and *CO compared to traditional d-block SACs.[4a,5] Unfortunately, the delocalized orbitals of main group SACs show an unsatisfactory ability of CO$_2$ activation to *COOH.[5a] Therefore, it is imperative to optimize the CO$_2$ activation process of main group SACs.

Many strategies have been employed to decrease the energy barrier of CO$_2$ activation for SACs, chiefly in the construction of low-coordination sites, diatomic structure, and heteroatomic coordination.[3a,6] For example, Jiang et al. designed Ni SAC with a low coordination number of 3 to promote electron localization and CO$_2$ activation for Ni sites,[7] leading to a prominent TOF of ≈1425 h^{-1}. In order to improve

Q. Wang, H. Li, K. Liu, J. Fu, W. Liao, S. Chen, M. Liu
Hunan Joint International Research Center for Carbon Dioxide Resource Utilization, State Key Laboratory of Powder Metallurgy, School of Physics and Electronics
Central South University
Changsha 410083, P. R. China
E-mail: minliu@csu.edu.cn
M. Dai, C. Ma, S. Zhang
College of Materials Science and Engineering
Hunan University
Changsha 410082, P. R. China

The ORCID identification number(s) for the author(s) of this article can be found under https://doi.org/10.1002/adma.202300695.

Y.-R. Lu, T.-S. Chan
National Synchrotron Radiation Research Center
Hsinchu 300, Taiwan
E. Pensa, E. Cortés
Nanoinstitute Munich, Faculty of Physics
Ludwig-Maximilians-Universität München
80539 München, Germany
E-mail: emiliano.cortes@lmu.de
Y. Wang, Y. Sun
School of Energy and Power Engineering
Beihang University
Beijing 100191, P. R. China
E-mail: sunif@buaa.edu.cn
Y. Sun
Research Center for Advanced Energy and Carbon Neutrality
Beihang University
Beijing 100191, P. R. China

electron localization and CO_2 activation, Lu et al. developed atomically dispersed Ni–Zn bimetal sites,[8] which exhibited a TOF of ≈1400 h^{-1}. However, the performance of SACs through these two strategies is still unappealing, because the electron density of metal sites is largely related to the species of coordination atoms.[9–12]

Herein, we localized electron on p-orbitals through an asymmetric coordination on Ca SAC (Ca-N_3O) by O doping to enhance the CO_2 activation. Density functional theory (DFT) calculations demonstrate the weaker adsorption of *CO and *H on Ca sites than that of Fe site. Ca-N_3O shows a facilitated *COOH formation process after O doping due to the electron localization induced by asymmetric coordination. The predicted theoretical results were proved experimentally. The Ca-N_3O catalyst was synthesized through a facile pyrolysis method and then structural characterizations such as X-ray absorption fine spectroscopy confirmed the Ca-N_3O catalyst with one O and three N coordination atoms anchored on nitrogen-oxygen co-doped carbon (NC). Owing to the O induced electron localization around Ca sites, the Ca-N_3O catalyst exhibits a turnover frequency (TOF) of ≈15 000 per hour in H-cell and a current density of −400 mA cm^{-2} with a CO Faradaic efficiency (FE) over 90% in flow cell. Additionally, Ca-N_3O remains a FE$_{CO}$ ≥ 90% even at a low CO_2 concentration. The favorable CO desorption of Ca SACs was confirmed by CO temperature programmed desorption (TPD). In situ attenuated total reflection infrared spectroscopy (ATR-IR) demonstrated that the transformation from *CO_2 to *COOH is favored on the Ca-N_3O and this is the pivotal step to enhance CO_2RR to CO.
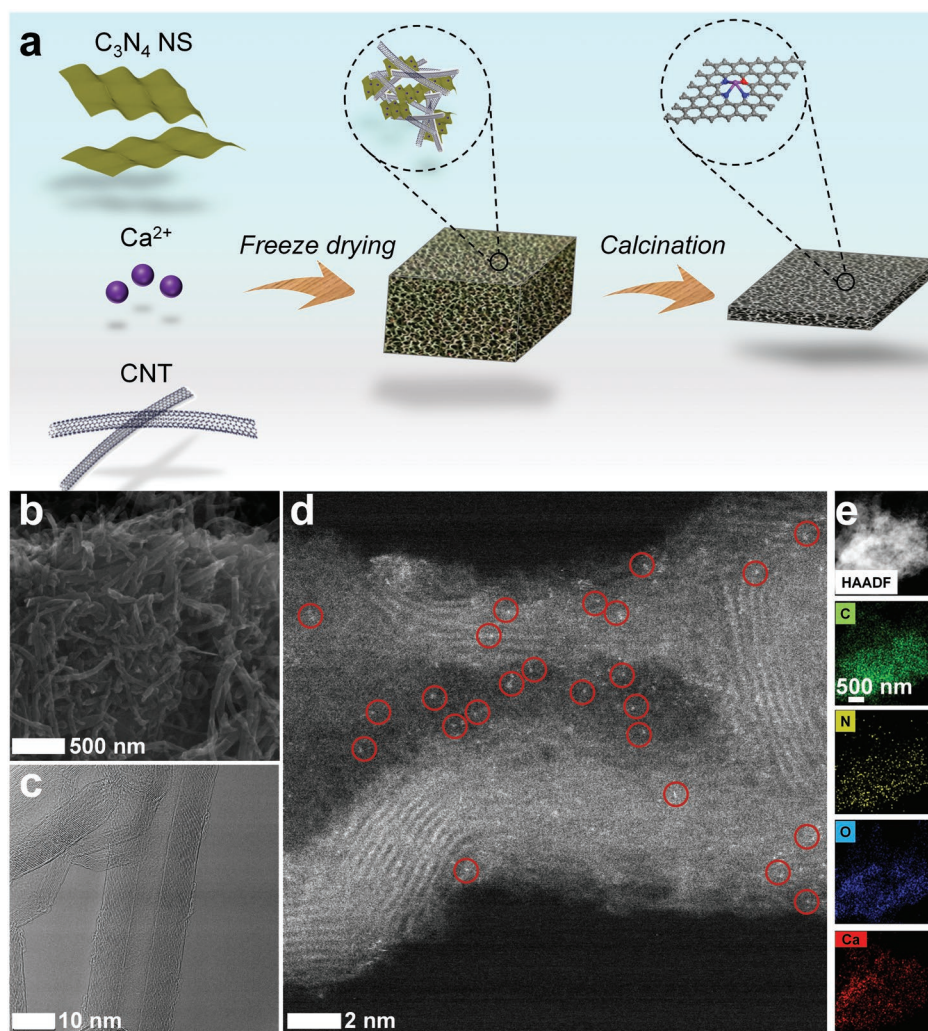
2. Results and Discussion

To figure out the difference between Ca SACs and a representative transition metal (i.e., Fe) SACs with d-orbitals, theoretical analyses based on DFT calculations were conducted (**Figure 1**a and Figure S1, Supporting Information). As shown in Figure 1b, the CO desorption energy barrier on Ca SACs (< 0 eV) is much lower than that on Fe-N_4 (1.38 eV). The energy barriers of HER on Ca SACs (>1.32 eV) are much higher than that on Fe-N_4 (−0.24 eV) (Figure 1c). These results indicate the p-orbitals of Ca sites are beneficial to inhibit both HER and CO poisoning, compared to d-orbitals of Fe sites.

In order to evaluate the effect of the asymmetric coordination on CO_2 activation, the theoretical simulations among Ca-N_3O and Ca-N_4 were analyzed. Mulliken charge analyses (Figure 1a and Table S1, Supporting Information) show that after the electron localization of Ca site by O doping, charge shift from Ca-N_3O to *COOH (0.74 e) is larger than that from Ca-N_4 (0.68 e).[13] Similarly, after *COOH formation, Ca-N_3O presents a larger shift of the p-band center (1.96 eV) than that of Ca-N_4 (1.08 eV) in the projected density of states (PDOS) (Figure 1d,e and Figure S2, Supporting Information), confirming more electrons in the p-orbitals of Ca-N_3O can be used to stabilize *COOH.[14] Adsorption energy analyses reveal the strong interaction between *COOH and Ca-N_3O (Figure 1f), which is confirmed by the lower energy barrier of *COOH from *CO_2 on Ca-N_3O (0.51 eV) compared with that on Ca-N_4 (0.59 eV) (Figure 1b). Moreover, adsorption energy analyses manifest all constructed Ca SACs (< 0.12 eV) exhibit much weaker adsorption of *CO than that of Fe SAC (2.34 eV), proving Ca SACs
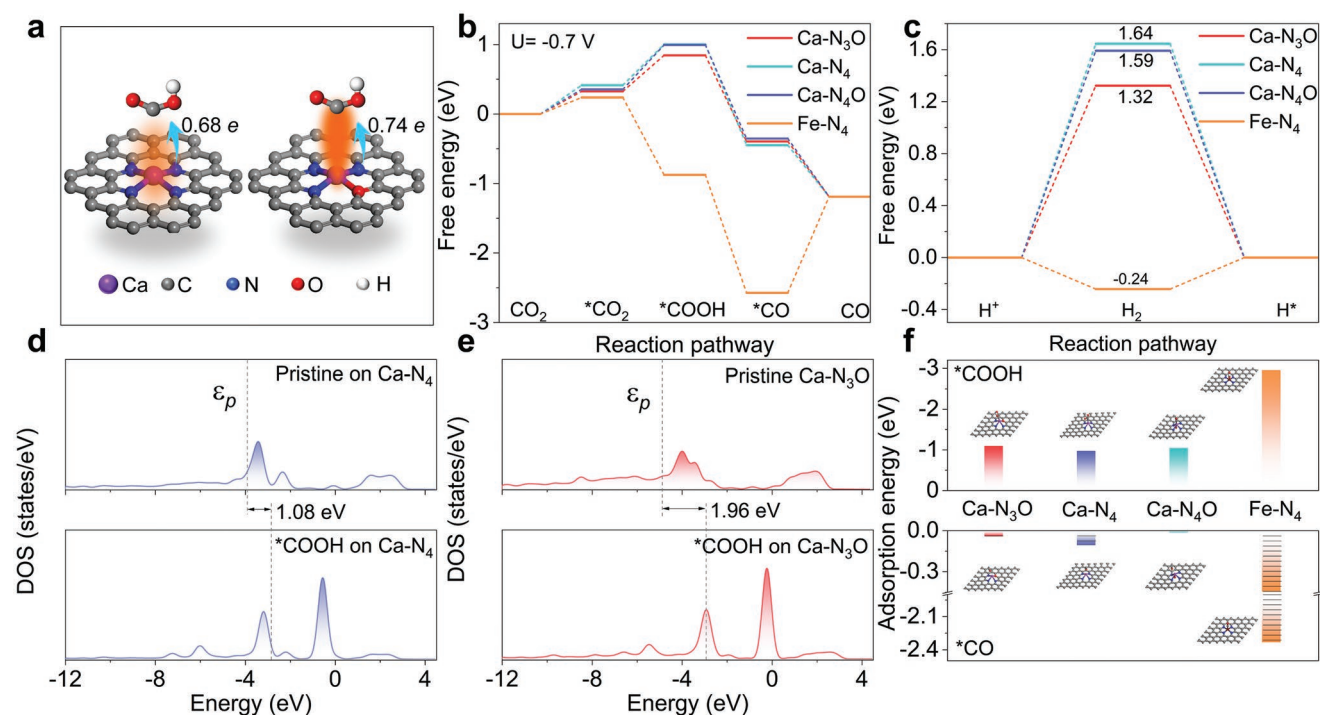
Figure 1. Theoretical calculations. a) Comparison of schematic diagram and Mulliken charge analysis for *COOH adsorbed on Ca-N_3O and Ca-N_4 orbitals. b,c) Free energy diagram for CO_2-to-CO conversion and hydrogen evolution. d,e) PDOS and p-band center (ε_p) for before and after *COOH adsorbed on Ca-N_4 and Ca-N_3O. f) Adsorption energy of *COOH and *CO on catalysts.

**ADVANCED
SCIENCE NEWS**

www.advancedsciencenews.com

**ADVANCED
MATERIALS**

www.advmat.de

Figure 2. a) Schematic illustration of the preparation for Ca-N$_3$O. b) SEM image for Ca-N$_3$O. c) HRTEM image for Ca-N$_3$O. d) AC HAADF-STEM image for Ca-N$_3$O. e) EDS maps for Ca-N$_3$O.

are beneficial for preventing CO poisoning. In addition, Ca SACs with symmetric five coordination atoms (Ca-N$_4$O) were further studied. The results show that Ca-N$_4$O has a higher energy barrier of *COOH formation than that on Ca-N$_3$O because increased coordination atoms capture more electrons from metal center.[7,15] Therefore, these results demonstrate that asymmetric Ca-N$_3$O possesses the electron localization on Ca site and effectively promotes the *COOH formation for CO$_2$RR to CO.

To prove the theoretical analyzation, Ca SACs were prepared through a pyrolysis method.[16] Briefly, salt-assisted method was used to synthesize C$_3$N$_4$ nanosheets (NS). Then the corresponding aerogels were acquired by the chelation between the functional groups (−NH$_2$, −CN) of C$_3$N$_4$ nanosheets and Ca or Fe ions (Figure S3, Supporting Information). Finally, the Ca SACs were obtained by pyrolysis of the aerogels (**Figure 2**a and Figure S4, Supporting Information). The contents of metal elements in Ca-N$_3$O, Ca-N$_4$O, and Fe-N$_4$ catalysts are 0.67, 0.64, and 1.02 wt%, respectively. No metal X-ray diffraction (XRD) and Raman signal could be found for Ca-N$_3$O, and Ca-N$_4$O

catalysts (Figures S5 and S6, Supporting Information), manifesting the absence of metallic phases and a good dispersion of the Ca atoms. Besides, according to inductively coupled plasma optical emission spectrometer analyses, any other metal contamination was not detected in the obtained SACs (Table S2 and Figure S7, Supporting Information).

Scanning electron microscope (SEM) and high-resolution transmission electron microscope (HRTEM) were used to investigate the morphology of Ca SACs (Figure 2b,c and Figures S8–S13, Supporting Information). The Ca atoms appearing as distributed bright spots were investigated with aberration-corrected high-angle annular dark-field scanning transmission electron microscopy (AC HAADF-STEM). No metal nanoparticle or cluster in Ca SACs was detected, confirming the good dispersion of Ca atoms. Furthermore, energy dispersive spectrometry (EDS) mappings reveal the uniform distribution of Ca species across the corresponding catalysts (Figure 2e; Figures S9 and S10, Supporting Information).

To explore the electronic structure of Ca SACs, high-resolution X-ray photoelectron spectroscopy (XPS) measurements
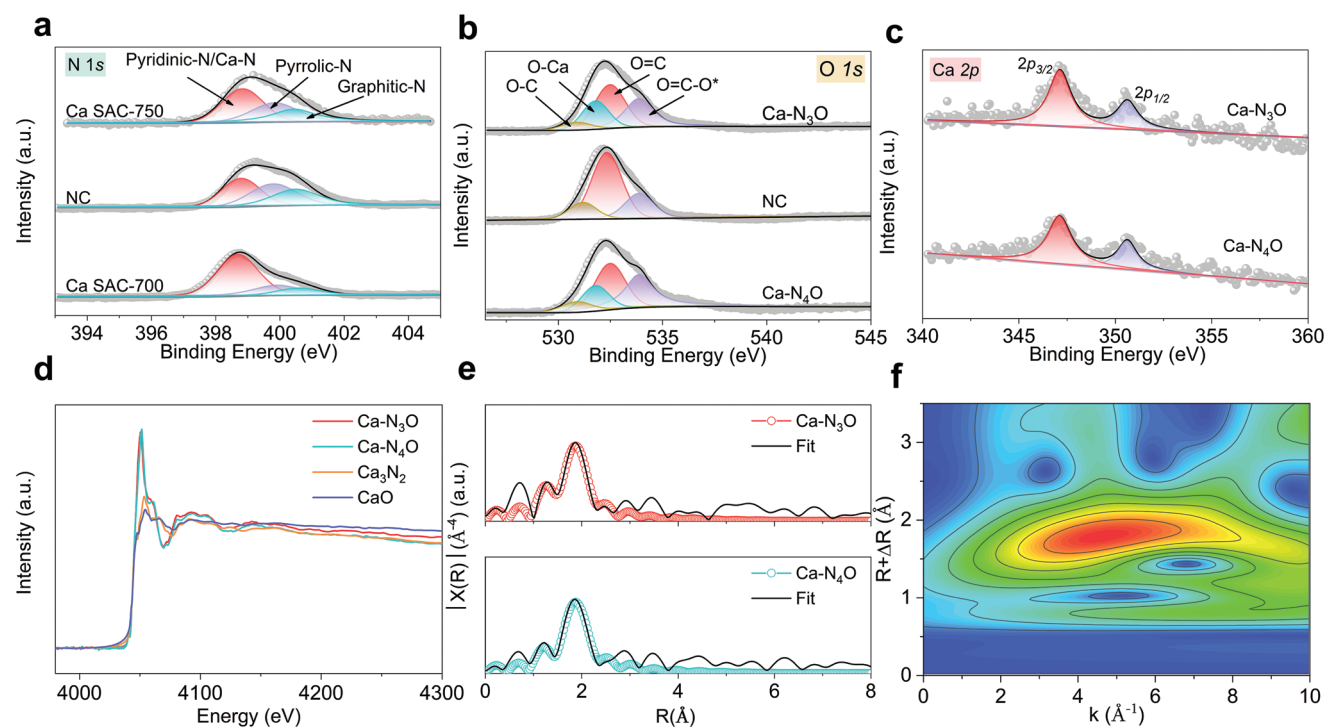
Figure 3. a–c) High-resolution XPS of N 1s, O 1s, and Ca 2p spectra of catalyst. d) Ca K-edge XANES spectra of catalysts. e) EXAFS fitting curves of catalyst. f) WT-EXAFS plot for Ca-N$_3$O.

were performed (Figure S14, Supporting Information). As shown in **Figure 3**a and Figure S15, Supporting Information, three peaks at about 400.8, 399.8, and 398.8 eV, deconvoluted from N 1s, can be assigned to the N atoms in graphitic-*N*, pyrrolic-*N*, and pyridinic-*N*/Ca-*N*, respectively.[17] The high-resolution O 1s peak of Ca SACs can be deconvoluted into four peaks, O═C─O (533.5 eV), O═C (532.5 eV), O─Ca (531.8 eV) and O─C (530.9 eV), indicating O atoms were successfully doped into the coordination environment (Figure 3b).[18] The peaks at 347.1 and 350.6 eV in the Ca 2p indicated that the Ca was presented in the form of +2 state due to N and O coordination (Figure 3c).[18] Combined with the deconvolution results of N 1s, O 1s, and Ca 2p spectra, it can be concluded that Ca─N and Ca─O coordination exist in the Ca-N$_3$O and Ca-N$_4$O catalysts.

To confirm the structure of catalysts, X-ray adsorption spectra (XAS) were performed (Figure 3d). The Ca K-edge X-ray adsorption near edge structure (XANES) spectra of Ca-N$_3$O and Ca-N$_4$O SAC are close to those of CaO and Ca$_3$N$_2$ references, indicating Ca presenting an oxidation state (Figure 3d). Fourier transformed extended X-ray adsorption fine structure (EXAFS) spectra reveal the atomically dispersed features of the Ca atoms in Ca-N$_3$O and Ca-N$_4$O SAC (Figure 3e and Figure S16, Supporting Information). From the fitting results of the EXAFS spectra, it can be found that there is no Ca─Ca bonding in Ca-N$_3$O and Ca-N$_4$O SAC, confirming the atomic dispersion feature of Ca atoms. The calculated N and O coordination numbers with central Ca atoms are ≈3 and ≈1 in Ca-N$_3$O, and ≈4 and ≈1 in Ca-N$_4$O, respectively, proving the structure features of the prepared samples (Table S3, Supporting Information).

High resolution wavelet transform (WT) EXAFS plots in K spaces further demonstrate the existence of Ca single atom configurations in catalysts (Figure 3f and Figure S17, Supporting Information). Atomic Fe-N$_4$ catalyst with ≈4 N coordination atoms is also confirmed by similar analyses (Figure S18 and Table S3, Supporting Information).

To assess the performance of catalysts, electrochemical tests were conducted in CO$_2$ saturated 0.5 м KHCO$_3$ (Figure S19, Supporting Information). No C$_2$ and liquid products but only CO and H$_2$ were detected from gas chromatograph and ^{1}H-NMR spectra (Figures S20-S23, Supporting Information). Remarkably, Ca-N$_3$O SAC exhibits the largest Faradaic efficiency of CO (FE$_{CO}$) of 97.3% at −0.85 V versus RHE, which is better than those of Ca-N$_4$O SAC (87.4% at −0.85 V) and Fe-N$_4$ SACs (67.6% at −0.95 V) (**Figure 4**a). It is worth mentioning that the potential with FE$_{CO}$ ≥ 90% of Ca-N$_3$O ranged from −0.65 to −1.05 V. The maximal partial current density of CO (J_{CO}) and TOF value with a FE$_{CO}$ ≥ 90% for Ca-N$_3$O SAC are 27 mA cm^{-2} and ≈15 000 h^{-1} at −1.05 V versus RHE in H-cell, respectively, which are far superior to those of Ca-N$_4$O SAC (18.6 mA cm^{-2}, ≈10 800 h^{-1}), Fe-N$_4$ SACs (11.8 mA cm^{-2}, ≈6000 h^{-1}) and those of other recently published works (Figure 4b; Figures S24–S26 and Table S4, Supporting Information).

To evaluate the potential practical applications, the flow cell with Ca-N$_3$O SAC was fabricated. It can be seen that Ca-N$_3$O SAC achieves a high current density of −400 mA cm^{-2} with an outstanding FE$_{CO}$ of ≈90% at −1.61 V and maintains stability at −100 mA cm^{-2} for over 26 h (Figure 4c,d and Figures S27,S28, Supporting Information). The performance under the dilute CO$_2$ was also conducted (Figure 4e and Figure S29, Supporting
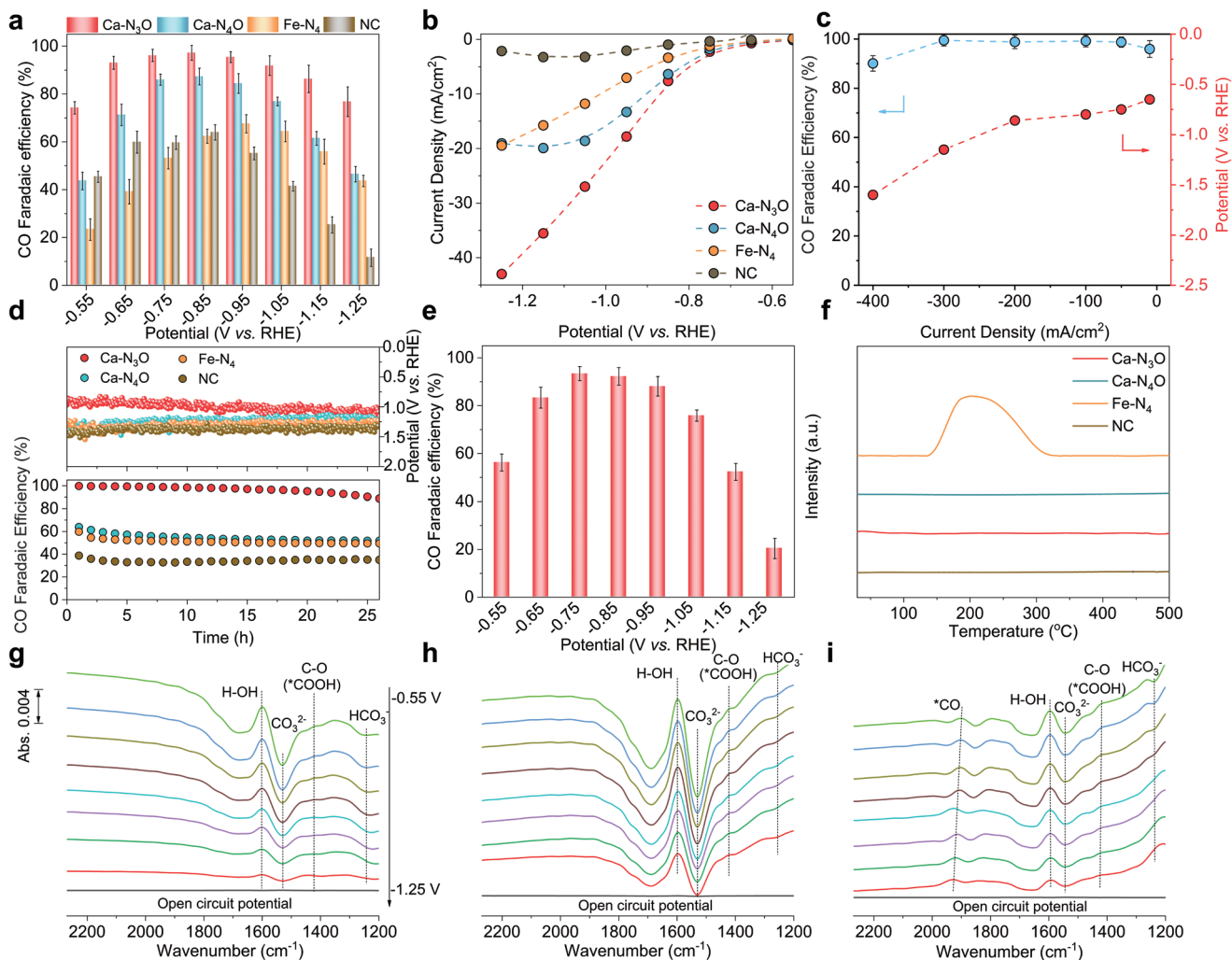
Figure 4. a) FE_{CO} at different potentials in H-cell. b) FE_{CO} and J_{CO} of catalysts. c) The potentials and FE_{CO} at different current densities of Ca-N$_3$O in flow cell. d) Stability of catalysts at a current density of −100 mA cm^{-2} in flow cell. e) FE_{CO} of Ca-N$_3$O at different potentials under 30% CO$_2$ concentration. f) CO TPD curves of catalysts. g–i) In situ ATR-IR spectra of Ca-N$_4$O, Ca-N$_3$O, and Fe-N$_4$.

Information), Ca-N$_3$O SAC still achieved a high current density with a FE_{CO} above 90% from −0.75 to −0.85 V versus RHE under the dilute CO$_2$ (30% CO$_2$ and 70% N$_2$). Therefore, Ca-N$_3$O SAC has an anticipated prospect in practical application.[19]

In order to explore the mechanism, CO TPD and in situ ATR-IR measurements were employed (Figure 4f–i and Figure S30, Supporting Information). CO TPD tests show that Ca-N$_3$O SAC possessed the largest CO deposition peak than those of other catalysts, indicating it has an outstanding property for CO deposition (Figure 4f). Raman peaks located at ≈1940, ≈1600, ≈1530, ≈1420, and ≈1250 cm^{-1} can be assigned to *CO stretching,[4a,20] H−O−H bending,[21] C=O (CO$_3^{2-}$) stretching,[22] C−O (*COOH) stretching[23] and HCO$_3^-$ stretching,[6a,22a] respectively (Figure 4g–i). Although CO was extensively generated, no distinct *CO peak on Ca-N$_3$O and Ca-N$_4$O SAC was found, manifesting CO was easily desorbed from Ca sites, which is consistent with the result of CO TPD test (Figure 4f). On the contrary, obvious *CO peaks were detected on Fe-N$_4$ catalyst (Figure 4i), revealing the strong CO

adsorption on Fe sites. Notably, the intensity of C−O (*COOH) stretching on Ca-N$_3$O SAC was larger than that of Ca-N$_4$O, indicating the facilitated *COOH formation on Ca-N$_3$O SAC. Thus, the results of TPD and in situ ATR-IR demonstrate that Ca-N$_3$O SAC exhibits a favorable *COOH formation and CO desorption, which is accordant with the DFT calculation results.

3. Conclusion

In summary, we developed a strategy to localize electron on p-orbitals of Ca through asymmetric coordination of Ca SAC (Ca-N$_3$O) by O doping, which enhances the CO$_2$ activation and thus the CO$_2$RR performance. Theoretical simulations prove that Ca sites on Ca SACs inhibit both HER and CO poisoning and the electron localization of Ca sites induced by O doping in Ca-N$_3$O could effectively promote the *COOH formation. To verify this theoretical prediction, we successfully synthesized asymmetric Ca-N$_3$O SAC, symmetric Ca-N$_4$O SAC, and

representative d-orbital Fe SACs. The targeted Ca-N$_3$O catalyst exhibits a state-of-the-art TOF of ≈15 000 per hour in H-cell and a current density of −400 mA cm^{-2} with a FE$_{CO}$ of ≈90% at −1.61 V in flow cell. Moreover, the FE$_{CO}$ of Ca-N$_3$O surpasses 90% even under dilute CO$_2$ concentration of only 30%. The results of in situ ATR-IR and CO TPD demonstrate the facile *COOH formation and CO desorption from the Ca-N$_3$O catalyst, which is consistent with our DFT results. Thus, our work provides a new insight into the regulation of atomically dispersed main group metal sites for CO$_2$RR.

Supporting Information

Supporting Information is available from the Wiley Online Library or from the author.

Conflict of Interest

The authors declare no conflict of interest.

Data Availability Statement

The data that support the findings of this study are available from the corresponding author upon reasonable request.

[1] a) X. Jiang, X. Nie, X. Guo, C. Song, J. G. Chen, *Chem. Rev.* **2020**, *120*, 7984; b) L. Wang, W. Chen, D. Zhang, Y. Du, R. Amal, S. Qiao, J. Wu, Z. Yin, *Chem. Soc. Rev.* **2019**, *48*, 5310; c) S. Zhang, Q. Fan, R. Xia, T. J. Meyer, *Acc. Chem. Res.* **2020**, *53*, 255; d) K. Li, J. Xu, T. Zheng, Y. Yuan, S. Liu, C. Shen, T. Jiang, J. Sun, Z. Liu, Y. Xu, M. Chuai, C. Xia, W. Chen, *ACS Catal.* **2022**, *12*, 9922.

[2] a) S. Jin, Z. Hao, K. Zhang, Z. Yan, J. Chen, *Angew. Chem., Int. Ed.* **2021**, *60*, 20627; b) M. Li, H. Wang, W. Luo, P. C. Sherrell, J. Chen, J. Yang, *Adv. Mater.* **2020**, *32*, 2001848; d) K. Li, S. Zhang, X. Zhang, S. Liu, H. Jiang, T. Jiang, C. Shen, Y. Yu, W. Chen, *Nano Lett.* **2022**, *22*, 1557.

[3] a) J. Zhu, M. Xiao, D. Ren, R. Gao, X. Liu, Z. Zhang, D. Luo, W. Xing, D. Su, A. Yu, Z. Chen, *J. Am. Chem. Soc.* **2022**, *144*, 9661; b) Y. Li, W. Shan, M. J. Zachman, M. Wang, S. Hwang, H. Tabassum, J. Yang, X. Yang, S. Karakalos, Z. Feng, G. Wang, G. Wu, *Angew. Chem., Int. Ed.* **2022**, *61*, e2022056; d) T. Ahmad, S. Liu, M. Sajid, K. Li, M. Ali, L. Liu, W. Chen, *Nano Res. Energy* **2022**, *1*, e9120021.

[4] a) Q. Wang, K. Liu, J. Fu, C. Cai, H. Li, Y. Long, S. Chen, B. Liu, H. Li, W. Li, X. Qiu, N. Zhang, J. Hu, H. Pan, M. Liu, *Angew. Chem., Int. Ed.* **2021**, *60*, 25241; b) T. Zhang, X. Han, H. Liu, M. Biset-Peiró, X. Zhang, P. Tan, P. Tang, B. Yang, L. Zheng, J. R. Morante, J. Arbiol, *Energy Environ. Sci.* **2021**, *14*, 4847.

[5] a) H. K. Lim, H. Shin, W. A. Goddard, Y. J. Hwang, B. K. Min, H. Kim, *J. Am. Chem. Soc.* **2014**, *136*, 11355; b) S. He, F. Ni, Y. Ji, L. Wang, Y. Wen, H. Bai, G. Liu, Y. Zhang, Y. Li, B. Zhang, H. Peng, *Angew. Chem., Int. Ed.* **2018**, *57*, 16114.

[6] a) M. Huang, B. Deng, X. Zhao, Z. Zhang, F. Li, K. Li, Z. Cui, L. Kong, J. Lu, F. Dong, L. Zhang, P. Chen, *ACS Nano* **2022**, *16*, 2110; b) C. Jia, X. Tan, Y. Zhao, W. Ren, Y. Li, Z. Su, S. C. Smith, C. Zhao, *Angew. Chem., Int. Ed.* **2021**, *60*, 23342.

[7] Y. Zhang, L. Jiao, W. Yang, C. Xie, H. L. Jiang, *Angew. Chem., Int. Ed.* **2021**, *60*, 7607.

[8] Y. Li, B. Wei, M. Zhu, J. Chen, Q. Jiang, B. Yang, Y. Hou, L. Lei, Z. Li, R. Zhang, Y. Lu, *Adv. Mater.* **2021**, *33*, 2102212.

[9] a) R. Qin, K. Liu, Q. Wu, N. Zheng, *Chem. Rev.* **2020**, *120*, 11810; b) X. Sun, Y. Tuo, C. Ye, C. Chen, Q. Lu, G. Li, P. Jiang, S. Chen, P. Zhu, M. Ma, J. Zhang, J. H. Bitter, D. Wang, Y. Li, *Angew. Chem., Int. Ed.* **2021**, *60*, 23614.

[10] Y. Wang, Q. Wang, J. Wu, X. Zhao, Y. Xiong, F. Luo, Y. Lei, *Nano Energy* **2022**, *103*, 107815.

[11] B. Zhang, J. Zhang, J. Shi, D. Tan, L. Liu, F. Zhang, C. Lu, Z. Su, X. Tan, X. Cheng, B. Han, L. Zheng, J. Zhang, *Nat. Commun.* **2019**, *10*, 2980.

[12] D. Zhao, K. Yu, P. Song, W. Feng, B. Hu, W. C. Cheong, Z. Zhuang, S. Liu, K. Sun, J. Zhang, C. Chen, *Energy Environ. Sci.* **2022**, *15*, 3795.

[13] L. Sun, Z. Huang, V. Reddu, T. Su, A. C. Fisher, X. Wang, *Angew. Chem., Int. Ed.* **2020**, *59*, 17104.

[14] S. Li, S. Zhao, X. Lu, M. Ceccato, X. M. Hu, A. Roldan, J. Catalano, M. Liu, T. Skrydstrup, K. Daasbjerg, *Angew. Chem., Int. Ed.* **2021**, *60*, 22826.

[15] Y. N. Gong, L. Jiao, Y. Qian, C. Y. Pan, L. Zheng, X. Cai, B. Liu, S. H. Yu, H. L. Jiang, *Angew. Chem., Int. Ed.* **2020**, *59*, 2705.

[16] a) C. Xia, Y. Qiu, Y. Xia, P. Zhu, G. King, X. Zhang, Z. Wu, J. Y. Kim, D. A. Cullen, D. Zheng, P. Li, M. Shakouri, E. Heredia, P. Cui, H. N. Alshareef, Y. Hu, H. Wang, *Nat. Chem.* **2021**, *13*, 887; b) Q. Wang, K. Liu, K. Hu, C. Cai, H. Li, H. Li, M. Herran, Y. R. Lu, T. S. Chan, C. Ma, J. Fu, S. Zhang, Y. Liang, E. Cortés, M. Liu, *Nat. Commun.* **2022**, *13*, 6082.

[17] Y. Li, X. F. Lu, S. Xi, D. Luan, X. Wang, X. W. Lou, *Angew. Chem., Int. Ed.* **2022**, *61*, e2022014.

[18] Z. Lin, H. Huang, L. Cheng, W. Hu, P. Xu, Y. Yang, J. Li, F. Gao, K. Yang, S. Liu, P. Jiang, W. Yan, S. Chen, C. Wang, H. Tong, M. Huang, W. Zheng, H. Wang, Q. Chen, *Adv. Mater.* **2021**, *33*, 2107103.

[19] H. L. Jiang, L. Jiao, W. Yang, G. Wan, R. Zhang, X. Zheng, H. Zhou, S. H. Yu, *Angew. Chem., Int. Ed.* **2020**, *59*, 20589.

[20] X. Qin, S. Zhu, F. Xiao, L. Zhang, M. Shao, *ACS Energy Lett.* **2019**, *4*, 1778.

[21] a) E. R. Corson, R. Kas, R. Kostecki, J. J. Urban, W. A. Smith, B. D. McCloskey, R. Kortlever, *J. Am. Chem. Soc.* **2020**, *142*, 11750; b) S. Zhu, T. Li, W. B. Cai, M. Shao, *ACS Energy Lett.* **2019**, *4*, 682.

[22] a) Y. Katayama, F. Nattino, L. Giordano, J. Hwang, R. R. Rao, O. Andreussi, N. Marzari, Y. Shao-Horn, *J. Phys. Chem. C* **2019**, *123*, 5951; b) M. F. Baruch, J. E. Pander, J. L. White, A. B. Bocarsly, *ACS Catal.* **2015**, *5*, 3148.

[23] a) X. Cao, L. Zhao, B. Wulan, D. Tan, Q. Chen, J. Ma, J. Zhang, *Angew. Chem., Int. Ed.* **2021**, *61*, e202113918; b) N. Firet, W. Smith, *ACS Catal.* **2016**, *7*, 606.